

ChemComm

Chemical Communications

Accepted Manuscript

This article can be cited before page numbers have been issued, to do this please use: Z. Hu, C. Yang, K. Lv, X. Li, Q. Li and J. Fan, *Chem. Commun.*, 2020, DOI: 10.1039/C9CC08578E.



This is an Accepted Manuscript, which has been through the Royal Society of Chemistry peer review process and has been accepted for publication.

Accepted Manuscripts are published online shortly after acceptance, before technical editing, formatting and proof reading. Using this free service, authors can make their results available to the community, in citable form, before we publish the edited article. We will replace this Accepted Manuscript with the edited and formatted Advance Article as soon as it is available.

You can find more information about Accepted Manuscripts in the [Information for Authors](#).

Please note that technical editing may introduce minor changes to the text and/or graphics, which may alter content. The journal's standard [Terms & Conditions](#) and the [Ethical guidelines](#) still apply. In no event shall the Royal Society of Chemistry be held responsible for any errors or omissions in this Accepted Manuscript or any consequences arising from the use of any information it contains.

COMMUNICATION

Single atomic Au induced dramatic promotion of the photocatalytic activity of TiO₂ hollow microspheresReceived 00th January 20xx,
Accepted 00th January 20xxZhao Hu^a, Chao Yang^a, Kangle Lv^{*a}, Xiaofang Li^b, Qin Li^a and Jiajie Fan^c

DOI: 10.1039/x0xx00000x

Single atomic Au (SA-Au) is firmly anchored on the surface of defective TiO₂ (DT) hollow microspheres with oxygen vacancy (Ov), which sharply improves the light-harvesting ability, stimulates the charge separation, and facilitates the adsorption and activation, therefore dramatically enhancing the photoreactivity towards acetone oxidation.

Up to now, TiO₂ is considered as the most typical semiconductor photocatalyst used for environmental remediation. However, the large bandgap and quick recombination of photo-generated electron-hole pairs hamper its practical applications.¹⁻⁸ To improve the photocatalytic activity of TiO₂, many strategies have been used such as doping TiO₂ with metal⁹ and nonmetal elements,¹⁰ coupling TiO₂ with other semiconductor photocatalyst to form heterojunction,¹¹ modifying TiO₂ with carbon materials,¹² transitional metals,¹³ or introducing surface defects.^{14,15} Recently, much work has been devoted to hollow structured TiO₂ photocatalysts, for example, TiO₂ hollow microspheres (TiO₂-HMSs), due to their unique properties such as good permeability, high efficient in light utilization, and convenience in filtering and recycling.¹⁶⁻¹⁸ To broaden the light-responsive range, we successfully prepared TiO₂-HMSs with surface oxygen vacancies (Ov) by simply calcination the mixture of pristine TiO₂-HMSs and urea, which exhibit overwhelming superior photocatalytic activity towards NO oxidation under the irradiation of a visible LED lamp.¹⁵

Now, single atomic catalysis is emerging as a new frontiers in (photo)catalysis. When compared with nanoparticles

deposited TiO₂ photocatalyst, isolated single atom modified TiO₂ usually exhibits superior photoreactivity due to the high ratio of coordination unsaturated surface atoms to overall atoms, which therefore can afford more sites to facilitate the interfacial reactions.^{2, 19,20} However, the high mobility of the single atoms makes them prefer to aggregate with each other to reduce the surface energy. Therefore, how to improve the stability of isolated single atomic site photocatalyst becomes a hot topic in photocatalysis, but it still remains a great challenge.^{21, 22}

Herein, we report a gentle method to prepare single atomic Au (Au-SA) anchored defective TiO₂-HMSs (DT) using surface oxygen vacancy (Ov) to stabilize Au-SA, and the photoreactivity of TiO₂-HMSs was evaluated by photocatalytic oxidation of acetone (setup in Fig. S1). For comparison, we prepared perfect TiO₂-HMSs (PT), Au nanoparticles modified PT (Au-NP/PT). The detailed processes for the synthesis of TiO₂ photocatalysts can be seen from the *supporting information*. We applied density functional theory (DFT) and *in-situ* diffuse reflectance infrared Fourier transform spectra (DRIFTS) spectrum to study the detailed oxidation processes of acetone over Au-SA/DT.

XRD characterization results show that all TiO₂-HMSs are pure anatase phase with a sharp peak at 2θ = 25.3° (Fig 1A), and only Au-NP/PT sample contains Au nanoparticles with two small diffraction peaks at 2θ = 38.2° and 44.4°. The absence of the diffraction peaks of Au nanoparticles for Au-SA/DT sample, suggesting that surface Ov of TiO₂ can be used to anchor single atomic Au. From the SEM (Fig. 1B) and TEM images (Fig. S2), we can see that these TiO₂-HMSs have similar morphology in diameters of about 2-3 μm, reflecting that the introduction of Ov and Au have little effect on the morphology of TiO₂-HMSs.

PT sample exhibits little absorption in visible region due to its large bandgap (Fig. 1C). After introduction of surface Ov, the absorption edge of TiO₂-HMSs (DT sample) extends to about 550 nm. The absorption of PT extends to the whole visible region after deposition of Au nanoparticles (Au-NP/PT sample), possibly caused by the localized surface plasmon resonance

^a Key Laboratory of Catalysis and Energy Materials Chemistry of Ministry of Education, College of Resources and Environmental Science, South-Central University for Nationalities, Wuhan, Hubei Province 430074, China.
E-mail: lvkangle@mail.scuec.edu.cn (K.L. Lv)
Tel: +86-27-67841369, Fax: +86-27-67843918

^b College of Chemistry and Chemical Engineering, Wuhan University of Science and Technology, Wuhan, 430081, China.

^c School of Materials Science and Engineering, Zhengzhou University, Zhengzhou 450001, China.

† Electronic Supplementary Information (ESI) available: Experimental section, characterization of the photocatalysts, nitrogen sorption, FTIR, TEM, EPR, XPS, PL, photocurrent, EIS, ESR, and DFT calculations. See DOI: 10.1039/x0xx00000x

(LSPR) effect.²³ Among all the TiO₂-HMSs, Au-SA/DT exhibits the strongest light-harvesting ability. According to the total DOS, the band gap of perfect TiO₂ (PT) is 2.2 eV (Fig. 1D), which is smaller than the experimental value due to the limitations of the known DFT method.²⁴ When compared with PT and DT, Au-SA/DT has the smallest bandgap due to the formed defect energy levels of the intermediate state, which therefore makes it possess the strongest light harvesting ability. The production of Ov in DT and Au-SA/DT photocatalysts is confirmed by ESR spectra (Fig. S3), where the Lorentzian line with the corresponding $g = 2.003$ stems from the Ov trapped electrons.^{25,26} Interestingly, the intensity of the signal for Ov is almost kept unchanged for DT even after anchoring of Au-SA.

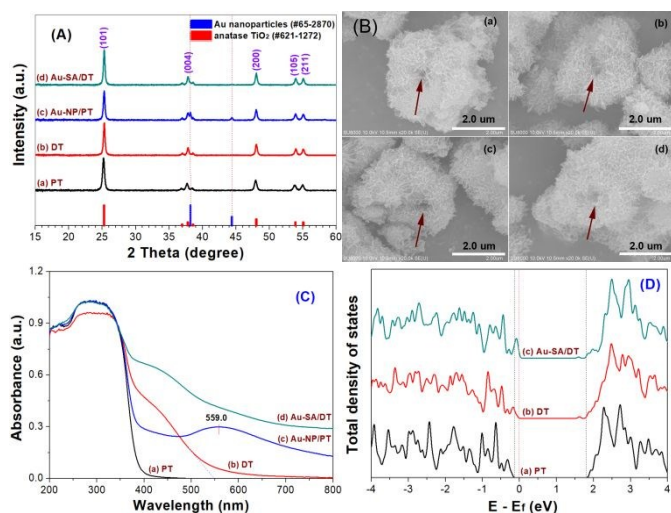


Fig. 1. XRD patterns (A), SEM images (B), diffuse reflectance spectra (C), and calculated total density of states (D) of the TiO₂-HMSs for perfect TiO₂ (PT), defective TiO₂ (DT), Au nanoparticle deposited TiO₂ (Au-NP/PT) and single atomic Au anchored TiO₂ (Au-SA/DT).

As expected, all samples have similar Brunauer-Emmett-Teller (BET) surface area (about 80-100 m²g⁻¹) and pore structures (Fig. S4 and Table S1). Therefore, BET surface area is not the key factors affecting the photoreactivity of TiO₂-HMSs. All the prepared TiO₂-HMSs contain Ti, O and small amount of C elements with binding energies of 458 (Ti 2p), 529 (O 1s) and 284 (C 1s), respectively (Fig. S5A). The C element is ascribed to the residual carbon from the adventitious hydrocarbon in XPS instrument itself.¹⁵ From the high resolution XPS spectra, we can see that both the binding energies of Ti 2p (Fig. S5B) and O 1s (Fig. S5C) reduce after introduction of Ov, which is due to the higher electronic density in Ov regions.¹⁵ The presence of Au in Au-SA/DT and Au-NP/PT samples are confirmed from the corresponding high resolution XPS spectra in Au 4f region (Fig. S5D), where two peaks with binding energies of 83.4 and 87.1 eV are corresponding to the orbital energies of Au 4f_{7/2} and Au 4f_{5/2}, respectively.²⁷

To disclose the fine structure and distribution of Au in Au-SA/DT sample, high-angle annular dark-field scanning TEM (HAADF-STEM) is performed. From Fig. 2a, we can observe the finely dispersed gold on the surface of TiO₂-HMSs. Surprisingly,

despite the relatively high Au loading (0.32 wt%, see Table S2) over DT, only atomically dispersed Au can be directly observed by aberration-corrected STEM (Fig. 2d), without the presence of any visible nanoparticles or clusters. On the contrary, from the HAADF-STEM and TEM images, we can clearly observe the presence of Au nanoparticles over Au-NP/PT sample (Figs. S6-S8). Then we can conclude that the Ov can be used to anchor atomically dispersed Au. From the X-ray absorption near-edge structure (XANES) spectra (Fig. 2e), we can find that the white line peak of Au-SA/DT is similar to that of HAuCl₄. From the extended X-ray absorption fine structure (EXAFS) spectra (Fig. 2f), we can compare the short-range local structure of Au. It can be clearly seen the Au-O shell ($R = 1.4$ Å) and Au-Ti shell ($R = 2.3$ Å) for Au-SA/DT sample. The Au-Au and Au-Cl coordination peaks are absent from the EXAFS spectra compared with Au foil and HAuCl₄, suggesting the absence of Au nanoparticles or clusters in Au-SA/DT sample, consistent with the HAADF-STEM observation (Fig. 2d).

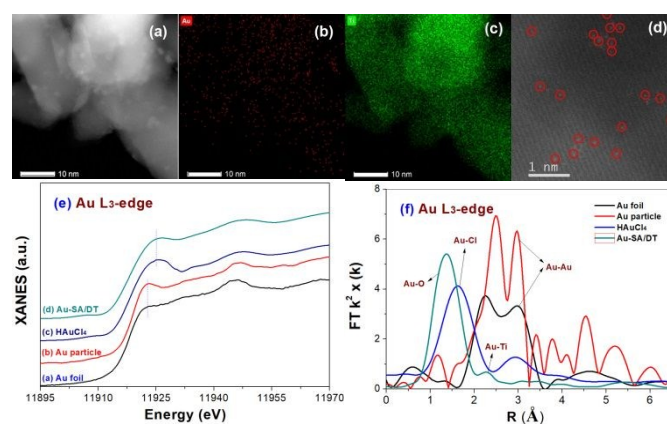


Fig. 2. HAADF-STEM image (a) and the corresponding element mappings for Au (b) and Ti (c) atoms of Au-SA/DT sample. Single atomic Au sites in HAADF-STEM image highlighted by red circles (d). L-edge XANES spectra (e) and R-space EXAFS magnitudes of TiO₂-HMSs (f).

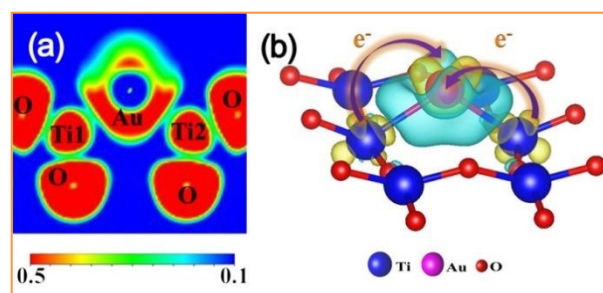


Fig. 3. The electronic local function (ELF) (a) and charge difference distribution of Au-SA/DT photocatalyst (charge accumulation in blue and charge depletion in yellow).

The electronic local function (ELF) result also supports the formation of Ti-Au-Ti bonds at the single atomic Au site (Fig. 3a). From the calculated charge difference distribution result, we can clearly see the electrons transfer from surrounding Ti to single atomic Au in Au-SA/DT photocatalyst, activating the single atomic Au due to the increased electronic density (Fig.

3b). The optimized atomic models of TiO₂ shows that the introduction of Ov results in a stretched length of neighboring Ti atoms (Ti1 and Ti2) that are around the Ov site from 3.77 to 4.73 Å. However, this distance slightly reduces to 4.49 Å after anchoring single atomic Au. That is to say, the anchored single atomic Au can stabilize the structure of defective TiO₂ (Fig. S9).

Photocatalytic oxidation of acetone under UV irradiation is used to evaluate the photoreactivity of the TiO₂-HMSs photocatalysts (Fig. 4A). It can be seen that the introduction of Ov or Au-NPs separately has little effect on the photoreactivity of TiO₂-HMSs towards acetone oxidation. However, the photoreactivity of DT greatly improves after anchored with Au-SA, exceeding that of PT by a factor of 3.1. The decomposed acetone soars from 67.8 ppm to 214.2 ppm within 60 min when Au-SA/DT is used as photocatalyst instead of PT (Fig. 4B). The photoreactivity of Au-SA/DT is also much higher than that of other photocatalyst. For example, only 90 ppm and 160 ppm of acetone can be decomposed when P25 TiO₂ and high-energy TiO₂ nanosheets are used as photocatalyst, respectively (Table S3). In addition, Au-SA/DT also exhibits excellent photostability. Its photocatalytic activity is almost kept unchanged even repeated used for 5 times (Fig. S10). We also systematically studied the effect of Au-SA loading amount on the photoreactivity of defective TiO₂-HMSs (Fig. S11). It can be seen that the photoreactivity of Au-SA anchored defective TiO₂-HMSs increases first and then decreases, and all Au-SA modified defective TiO₂-HMSs exhibit higher photoreactivity than Au-NP/PT photocatalyst.

DFT calculation results show the adsorption energy of acetone over Au-SA/DT is -0.41 eV, much larger than that over PT (-0.30 eV) and DT samples (-0.23 eV), which indicate that Au-SA/DT exhibits stronger adsorption to acetone when compared with PT and DT photocatalysts (Fig. S12). The stronger adsorption will facilitate the activation of acetone. Larger Bader charge (-0.04 e) of the adsorbed acetone over Au-SA/DT is observed than that over PT (-0.01 e) and DT photocatalysts (-0.02 e).

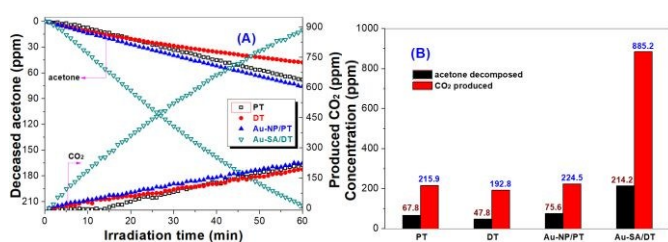


Fig. 4. Photocatalytic oxidation of acetone over different TiO₂-HMSs (A) and comparison of the photoreactivity (B).

Ov can act as an electron trap. Then, it is not strange to see a reduced photoluminescence (PL) intensity of DT than that of PT (Fig. S13A). When compared with Au-NP/PT, Au-SA/DT sample possesses lower PL intensity, which infers that the introduction of SA-Au can sharply retards the recombination of photo-generated carriers, improving the photoreactivity. The retarded recombination of carriers is further confirmed by transient PL spectra (Fig. S13B). The average lift time of the

carriers are 1.13, 2.34, 1.96 and 2.67 ns for PT, DT, Au-NP/PT and Au-SA/DT sample, respectively (Table S11). The longest average life time of the carriers for Au-SA/DT also indicates the severely retarded recombination of carriers. As Au-SA/DT photocatalyst exhibits the strongest light-harvesting ability (Fig. 1C) and has the longest average life time of photo-generated carriers (Fig. S13B), it is not hard to understand the superior photocatalytic activity of Au-SA/DT among all the photocatalysts. Consistent with the results of PL spectra, Au-SA/DT photocatalyst performs the highest photocurrent (Fig. S13C) and smallest arc radius on the Nyquist plot in the high frequency range of the electrochemical impedance spectroscopy (Fig. S13D), suggesting its quickest interfacial charge transfer to the electron donor/acceptor.

Both hydroxyl radicals ($\bullet\text{OH}$) and superoxide radicals ($\bullet\text{O}_2^-$) are important reactive oxygen species (ROSS) that are responsible for the oxidation of organic pollutants.^{5,7,8} Here we performed the radicals-trapping experiments (Fig. S14). Under UV irradiation for 5 min, both the signals of the DMPO trapped $\bullet\text{OH}$ and $\bullet\text{O}_2^-$ radicals in suspensions of PT and DT are very weak. However, after loading TiO₂-HMSs with Au-NP and Au-SA, the intensities of the signals for the trapped $\bullet\text{OH}$ and $\bullet\text{O}_2^-$ radicals greatly improve, and Au-SA/DT exhibits the strongest signals, suggesting its excellent photocatalytic activity.

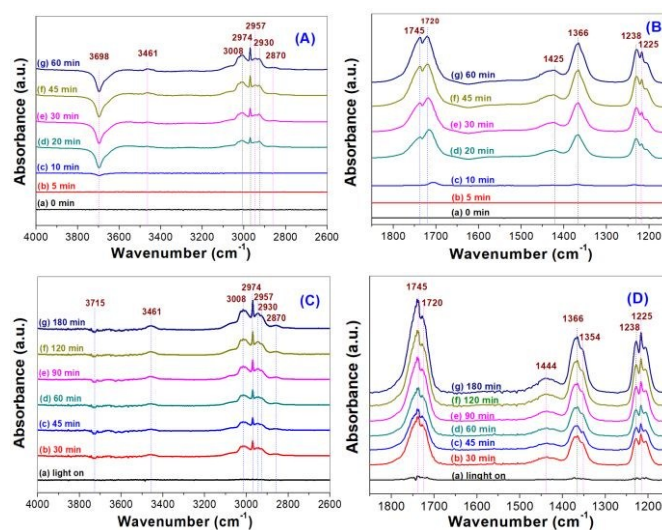


Fig. 5. *In-situ* DRIFTS recording the adsorption (A and B) and photocatalytic oxidation process (C and D) of acetone over Au-SA/TiO₂ under a mixed gas flow of acetone and O₂.

The time dependent dark adsorption of acetone over Au-SA/DT is recorded by *in-situ* DRIFTS (Fig. 5A and Fig. 5B), where the negative bands at 3698 cm⁻¹ is related to the depletion of adsorbed acetone, and the positive bands at 3008, 2974, 2957, 2930, 1366 and 1238 cm⁻¹ are corresponding to the molecularly adsorbed acetone.²⁸ The peak at 1720 cm⁻¹ can be assigned to the $\nu(\text{C}=\text{O})$ vibration mode of adsorbed aldehyde.²⁹ Both formaldehyde and acetaldehyde are plausible intermediates of acetone photocatalytic oxidation, and they could account for the band at 2870 cm⁻¹ which is characteristic of the $\nu(\text{CH})$ vibration of aldehyde molecules. Therefore,

acetaldehyde is very likely to form during adsorption acetone. The peak centering at 1745 cm^{-1} could correspond to formic acid. However, the possible formation of acetic acid cannot be ascertained, because the corresponding $\nu(\text{CO})$ band overlaps with that of the acetone. In addition, we can observe the typical IR absorption peak of bicarbonates featuring at 1225 cm^{-1} . Consequently, we can conclude the oxidation of acetone over Au-SA/DT photocatalyst occurs in the dark. The assignments of the absorption peaks are shown in Table S4.

After establishment of the adsorption equilibrium, the photocatalytic oxidation of acetone begins, and the *in-situ* DRIFTS recording the reaction of acetone over Au-SA/DT under UV irradiation are displayed in Fig. 5C and Fig. 5D. Although most of the DRIFTS during photocatalytic reaction are similar to these of adsorption process, some peaks become much stronger such as the peak centering at 1745 cm^{-1} , indicating a rapid accumulation of formic acid. In order to verify the above conclusions, we calculated the reaction path of acetone over Au-SA/DT photocatalyst and the corresponding reaction energy is obtained using Dmol3 module. Fig. S15 presents the changes of the free energy in reactions, from which we can see that the rate-determining step (RDS) for acetone oxidation is the decomposition of formic acid with an energy barrier of 1.22 eV. The reactions involved in acetone oxidation are listed in Table S5. Based on the *in-situ* DRIFTS and calculation, we proposed the oxidation pathway of acetone over Au-SA/DT photocatalyst (Fig. S16), including the excitation of TiO_2 photocatalyst to form ROSs, the adsorption and oxidation of acetone to produce acetic acid and formaldehyde. The decarboxylation of the acetic acid results in the formation of methyl, which can also transform into formaldehyde. Under the attacks of ROSs, formaldehyde is further oxidized into formic acid, and finally decomposes into CO_2 .

In summary, Ov is used to anchor and stabilize the single atomic Au on the surface of TiO_2 -HMSs (Au-SA/DT). The formation of Ti-Au-Ti bond facilitates the electron transfer from Ti to Au, resulting in an increased adsorption and activation of acetone. The photocatalytic activity of Au-SA/DT hollow microspheres is much higher than that of perfect TiO_2 -HMSs (PT), defective TiO_2 -HMS (DT) and even Au nanoparticles deposited perfect TiO_2 -HMSs (Au-NP/PT). The degradation pathway of acetone on the surface of Au-SA/DT is proposed based on the *in-situ* DRIFTS and DFT calculation. Au-SA/DT photocatalyst has the merits of good permeability, strong light-harvesting ability, broad light-responsive range and excellent photo-stability, which makes it promising to be practically used for air purification.

This work was supported by the National Natural Science Foundation of China (51672312, 21571192 & 21373275) and the Fundamental Research Funds for the Central Universities, South - Central University for Nationalities (CZT18016).

Conflicts of interest

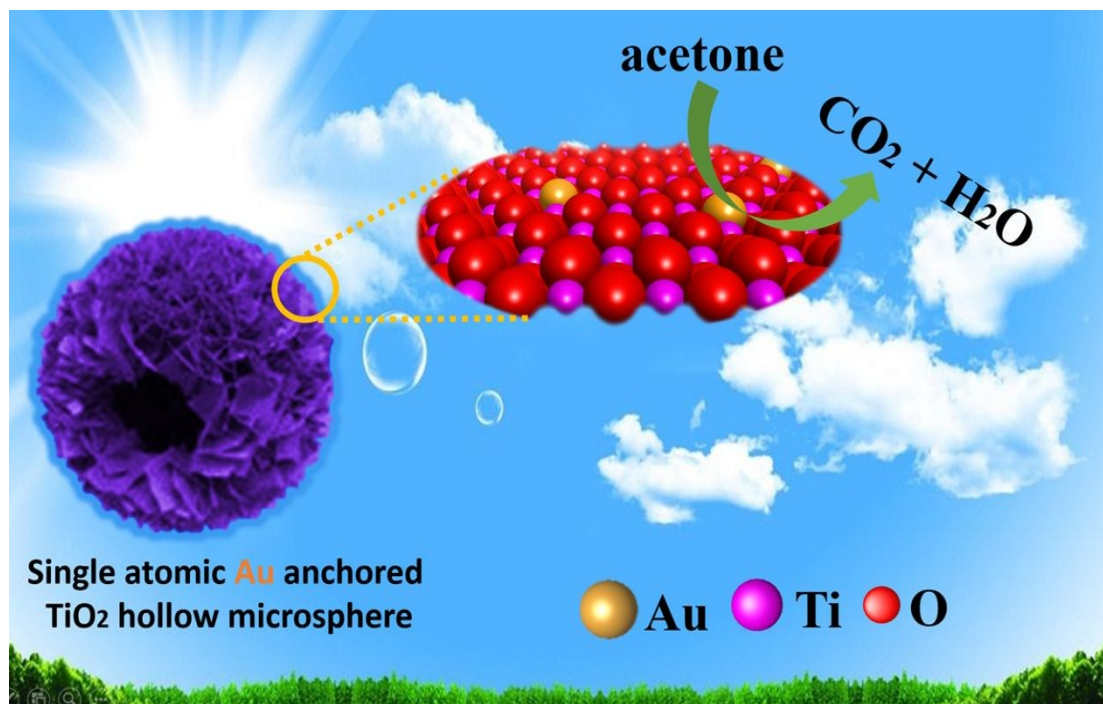
There are no conflicts to declare.

Notes and references

View Article Online

DOI: 10.1039/C9CC08578E

- 1 T.R. Gordon, M. Cargnello, T. Paik, F. Mangolini, R.T. Weber, P. Fornasiero and C.B. Murray, *J. Am. Chem. Soc.*, 2012, **134**, 6751-6761.
- 2 S. Saurabh, P.T. Joseph, M.A. Rahman, M. Abd-Ellah, M. Mohapatra, P. Debabrata, N.F. Heinig and K.T. Leung, *ACS Nano.*, 2014, **8**, 11891-11898.
- 3 L. Zhang, C. Yang, K. L. Lv, Ya. C. Lu, Q. Li, X. F. Wu, Y. Y. Li, X. F. Li, J. J. Fan and M. Li, *Chin. J. Catal.*, 2019, **40**, 755-764.
- 4 J. S. Cheng, Z. Hu, L. Lv, X. F. Wu, Q. Li, Y. H. Li, X. F. Li and J. Sun, *Appl. Catal. B: Environ.*, 2018, **232**, 330-339.
- 5 H. Sakurai, M. Kiuchi, C. Heck and T. Jin, *Chem. Commun.*, 2016, **52**, 13612-13615.
- 6 T. Jin, C. Liu and G. H. Li, *Chem. Commun.*, 2014, **50**, 6221-6224.
- 7 S. W. Liu, J. G. Yu, and M. Jaroniec, *J. Am. Chem. Soc.*, 2010, **132**, 11914-11916.
- 8 S. W. Liu, J. Q. Xia, and J. G. Yu, *ACS Appl. Mater. Interfaces.*, 2015, **7**, 8166-8175
- 9 S.K. Pathak, A. Abate, P. Ruckdeschel, B. Roose, K.C. Gödel, Y. Vaynzof, A. Santhala, S-I. Watanabe, D.J. Hollman, N. Noel, A. Sepe, U. Wiesner, R. Friend, H.J. Smith and U. Steiner, *Adv. Funct. Mater.*, 2014, **24**, 6046-6055.
- 10 M.P. Suryawanshi, U.V. Ghorpade, S.W. Shin, M.G. Gang, X.M. Wang, H. Park, S.H. Kang and J.H. Kim, *ACS Catal.*, 2017, **7**, 8077-8089.
- 11 K. Li, B. Chai, T.Y. Peng, J. Mao and L. Zan, *ACS Catal.*, 2013, **3**, 170-177.
- 12 S.L. Wang, J. Li, S.J. Wang, J. Wu, T.I. Wong, M.L. Foo, W. Chen, K. Wu and G.Q. Xu, *ACS Catal.*, 2017, **7**, 6892-6900.
- 13 J.M. Valero, S. Obregón and G. Colón, *ACS Catal.*, 2014, **4**, 3320-3329.
- 14 H. Shang, M.Q. Li, H. Li, S. Huang, C.L. Mao, Z.H. Ai and L. Z. Zhang, *Environ. Sci. Technol.*, 2019, **53**, 6444-6453.
- 15 Z. Hu, K.N. Li, X.F. Wu, N. Wang, X.F. Li, Q. Li, L. Li and K. L. Lv, *Appl. Catal. B: Environ.*, 2019, **256**, 117860.
- 16 Q. Li, Y. Xia, C. Yang, K.L. Lv, M. Lei and M. Li, *Chem. Eng. J.*, 2018, **349**, 287-296.
- 17 G.D. Moon, J.B. Joo, M. Dahl, H.J. Jung and Y.D. Yin, *Adv. Funct. Mater.*, 2014, **24**, 848-852.
- 18 J.B. Joo, I. Lee, M. Dahl, G.D. Moon, F. Zaera and Y.D. Yin, *Adv. Funct. Mater.*, 2013, **23**, 4246-4250.
- 19 X. Chen, L. Liu, P. Yu and S.S. Mao, *Science.*, 2011, **331**, 746-801.
- 20 P.P. John, B. Kieron and M. Ernzerhof, *Phys Rev. Lett.*, 1996, **77**, 3865-3868.
- 21 J.W. Wan, W.X. Chen, C.Y. Jia, L.R. Zheng, J.C. Dong, X.S. Zheng, Y. Wang, W.S. Yan, C. Chen, Q. Peng, D.S. Wang and Y.D. Li, *Adv Mater.*, 2018, 1705369.
- 22 G. Kresse and J. Furthmüller, *Computa. Mat. Sci.*, 1996, **6**, 15-15125.
- 23 L. Hou, M. Zhang, Z. Guan, Q.W. Li and J. Yang, *Appl. Sur. Sci.*, 2018, **428**, 640-647.
- 24 P.E. Blochl, *Phys. Rev. B*, 1994, **50**, 17953-17979.
- 25 M.P. Mani Prabha Singh and G.F. Strouse, *J. Am. Chem. Soc.*, 2010, **132**, 9383-9391.
- 26 Z. Tian, H. Cui, G. Zhu, W. Zhao, J. Xu, F. Shao, J. He and F. Huang, *J. Power Sources.*, 2016, **325**, 697-705.
- 27 M.P. Casaletto, A. Longo, A. Martorana, A. Prestianni and A.M. Venezia, *Surf. Interface Anal.*, 2006, **38**, 215-218.
- 28 M. El-Maazawi, A. N. Finken, A. B. Nair and V. H. Grassian, *J. Catal.*, 2000, **191**, 138-146.
- 29 E. Rekoske and M. A. Barteau, *Langmuir.*, 1999, **15**, 2061-2070.



Surface oxygen vacancy (Ov) is used to stabilize single atomic Au on the surface of TiO₂ hollow microspheres (TiO₂-HMSs), sharply improving its photoreactivity towards acetone oxidation.